American Mineralogist, Volume 81, pages 1249–1262, 1996

High-precision analysis of hydrous rhyolitic glass inclusions in quartz phenocrysts using the electron microprobe and INAA

BENJAMIN HANSON,[1,*] JOHN W. DELANO,[1] AND DAVID J. LINDSTROM[2]

[1]Department of Geological Sciences, University at Albany, State University of New York, Albany, New York 12222, U.S.A.
[2]Planetary Materials Branch, SN4/NASA Johnson Space Center, Houston, Texas 77058, U.S.A.

ABSTRACT

A high-precision electron microprobe (EMP) technique has been developed that is capable of analyzing major, minor, and trace element abundances (Si, Ti, Al, Fe, Mn, Mg, Ca, Na, K, Cl) in hydrous rhyolitic glasses. The technique was developed to characterize the chemical compositions of rhyolitic glass inclusions in phenocrysts that occur in layers of Paleozoic altered volcanic ash. The compositions of these inclusions serve as excellent chemical "fingerprints" of the altered volcanic ash layers for use in stratigraphic correlation. The precision and reproducibility of the analyses is sufficient not only to distinguish one altered volcanic ash layer from another on the basis of inclusion compositions, but also to discern differences in the compositions of different inclusions from the same layer. A high-precision instrumental neutron activation analytical (INAA) technique was also developed that is capable of measuring an additional suite of trace elements (e.g., Sc, Co, Rb, Cs, Sr, Ba, La, Ce, Sm, Eu, Tb, Yb, Lu, Zr, Hf, Ta) in rhyolitic glass inclusions in quartz phenocrysts with excellent accuracy and precision after correcting for the presence of the host quartz. The abundances of elements measured by the EMP technique and the corrected abundances determined using the INAA technique are identical within analytical uncertainty, thus demonstrating the internal consistency of the results.

INTRODUCTION

Silica-rich rhyolitic glass inclusions in quartz crystals (Fig. 1) have recently been found in highly altered volcanic ash layers (bentonitic tephras) that occur in Late Ordovician and Early Devonian sedimentary rocks from the northeastern U.S. (Schirnick 1990; Hanson et al. 1992a, 1992b; Delano et al. 1994; Mitchell et al. 1994). These glass inclusions have remained unaltered since early Paleozoic time because they are hermetically sealed in chemically resistant phenocrysts, which have protected them from chemical alteration by diagenetic fluids during the bentonitization process. The inclusions are samples of rhyolitic melt that became trapped during phenocryst growth in the preeruptive magma chamber and were quenched to glass during explosive eruption.

Bentonitic tephras are ideal for use as correlative timelines in stratigraphy (e.g., Sardeson 1928) because they represent geologically instantaneous events (volcanic airfall) that occur on the scale of days. That use, however, depends critically on being able to distinguish uniquely one bentonitic tephra from another. In the past, bentonitic tephra layers were correlated by a variety of methods. The more convincing of these correlation techniques attempted to characterize chemically the bentonitic tephras on the basis of the bulk composition (e.g., Huff 1983; Huff and Kolata 1989), the compositions of phenocrysts (e.g., Samson et al. 1995; Haynes 1994; Haynes et al. 1995), or the compositions of glass inclusions in phenocrysts (e.g., Delano et al. 1994; Mitchell et al. 1994; Lyons et al. 1992) from the bentonitic tephras. A reliable "fingerprint" of an individual eruption, however, can be obtained only if the deposit was not affected by posteruptive processes such as diagenesis or mixing of the bentonitic tephras with sediment by bioturbation. This problem may be particularly acute in the case of thin layers (e.g., ≤ 1 cm). The glass inclusions in chemically resistant phenocrysts from bentonitic tephras offer ideal chemical fingerprints because they are samples of melt trapped during phenocryst growth in the magma chamber prior to eruption. For the elements of interest in the current investigation, these glass inclusions have remained chemically closed systems since their entrapment.

The use of glass inclusions in chemical fingerprinting depends on the investigator's ability to analyze the glass with sufficient accuracy and precision so that different bentonitic tephra layers can be confidently distinguished. This task is complicated by the fact that most of the elements that show enough variation to be useful in chemical fingerprinting of rhyolitic glasses occur at minor and trace element levels. Obtaining high-precision electron microprobe analyses on minor and trace elements is further complicated by the presence of alkalis. Both K_2O

* Present address: Planetary Materials Branch, SN4/NASA Johnson Space Center, Houston, Texas 77058, U.S.A.

0003-004X/96/0910-1249$05.00

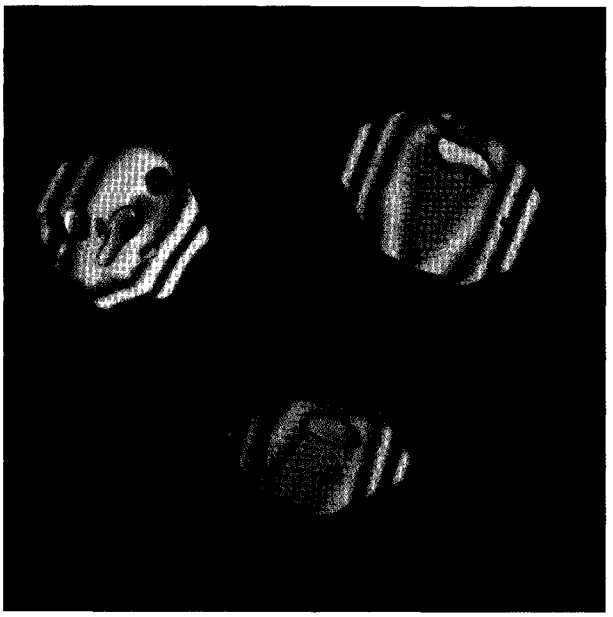

FIGURE 1. Photomicrograph of euhedral quartz phenocrysts measuring up to 250 μm across containing rhyolitic glass inclusions. These crystals, from a Middle Ordovician K-bentonite in Canajoharie, New York, are in immersion oil (RI = 1.5150) and were photographed in cross-polarized light with a gypsum plate inserted. For EMP analyses, crystals were mounted in epoxy, sectioned, and polished to expose the glass inclusions at the surface.

and Na_2O occur in major element abundances and are known to be mobile during exposure to the electron beam (e.g., Rutherford et al. 1985; Jercinovic and Keil 1988).

Electron microprobe analysis typically has been used to determine the major element compositions of rhyolitic glass inclusions (e.g., Takenouchi and Imai 1975; Beddoe-Stephens et al. 1983; Rutherford et al. 1985; Payette and Martin 1986; Webster and Duffield 1991; Lyons et al. 1992; Rutherford and Devine 1993; Dunbar and Kyle 1993). Secondary ion mass spectrometry (SIMS) has also been successfully used to determine the abundances of minor and trace elements in rhyolitic glasses, as well as H_2O (e.g., Hervig et al. 1989; Webster and Duffield 1991; Hervig and Dunbar 1992; Dunbar and Hervig 1992a, 1992b; Lu et al. 1992; Dunbar and Kyle 1993; Webster et al. 1995; Devine et al. 1995).

This contribution provides detailed descriptions of electron microprobe and high-sensitivity instrumental neutron activation analysis (INAA) techniques that have been developed to obtain precise and accurate minor and trace element data for chemical fingerprinting in stratigraphic studies and detailed petrogenetic investigations of melt compositions. Because these techniques provide reliable analyses for single inclusions, compositional variations within populations of glass inclusions from single bentonitic tephras can be determined.

Various microbeam techniques are now available that are capable of analyzing minor and trace element abundances with comparable or higher precision than the electron microprobe techniques described in this contribution (e.g., ion microprobe or laser-ablation inductively coupled mass spectrometry). These microbeam techniques may also be far less time consuming than the techniques described below. Electron microprobes, on the other hand, are far more abundant, less expensive to operate, and more readily accessible to most geologists than any of these other spot techniques, and they offer excellent spatial resolution (e.g., Devine et al. 1995). Although the INAA technique described below is time-consuming and the low-background counting facilities are rare, the abundances of a large set of elements can be determined for each crystal in a single analytical session. Furthermore, if several tens of samples are irradiated and counted in a single session, a large amount of highly precise and accurate data can be obtained efficiently.

Glass inclusions in quartz phenocrysts from a single K-rich bentonitic tephra (K-bentonite) collected from an outcrop of the Middle Ordovician Utica Formation along the Otsquago Creek, Schenectady County, New York (Mitchell et al. 1994), were analyzed as a demonstration of the methods. This K-bentonite is referred to as the "Otsquago Creek bentonite" in the following discussion. The calcareous black shales of the Utica Formation were deposited in a foreland basin during the Taconic Orogeny (e.g., Rowley and Kidd 1981).

SAMPLE PREPARATION

Samples of bulk nonlithified bentonitic tephras were washed through a sieve, and the fraction >105 μm was retained. This fraction was then treated with either hydrochloric or nitric acids (of varying concentrations) to remove clays adhering to the phenocrysts. The acid was then neutralized by dilution, decanted, and the coarse material was resieved. This process removed most of the adhering materials from the phenocrysts. The remaining material was dried and placed in a Frantz isodynamic magnetic separator to concentrate the quartz phenocrysts. The material was then placed in immersion oil (refractive index of 1.5150) and examined under a binocular microscope at 72× magnification. Phenocrysts that contained glass inclusions were hand-picked, individually mounted in epoxy, ground, and polished for electron microprobe analysis. Further preparation of phenocrysts for instrumental neutron activation analysis (INAA) is discussed below.

ELECTRON MICROPROBE ANALYSES

Analyses for major and minor elements were obtained using a JEOL 733 Superprobe located at the Department of Earth and Environmental Sciences at Renssalaer Polytechnic Institute. The instrument was equipped with five wavelength-dispersive spectrometers and on-line data reduction. Each glass inclusion was analyzed using three separate packages of five elements in a series of three steps. The five-element packages are as follows: package 1 = Na, K, Al, Si, and Fe; package 2 = Mg, Ti, Al, Cl,

and Fe; package 3 = Mg, Ca, Al, Mn, and Fe. During an analytical session, all glass inclusions were analyzed for one package of five elements before moving on to the next analytical step. During each analysis, each spectrometer was dedicated to one element for the entire analysis (Table 1). For minor and trace elements, backgrounds were collected on every analysis. Because the major element composition of rhyolitic glass inclusions in quartz is nearly constant, a set of ZAF matrix corrections was stored in the computer and applied to element packages 2 and 3. Typical minor and trace element abundances were stored and applied to the results of element package 1. The five-element packages represent partial analyses of the rhyolitic glasses. The combined results from the three five-element packages provide a "complete" analysis.

The first step of the analysis of a rhyolitic glass inclusion involves analysis of Na_2O, K_2O, Al_2O_3, SiO_2, and FeO, which are all present in major element abundances. (Although Fe is measured in the first five-element package, the operating conditions make the quality of its analysis inferior to Fe abundances determined in the next two analytical sequences.) Part of the uncertainty in the analysis of major elements arises from mechanical imperfections in the gears and stepper motors of the spectrometers. This source of error can be eliminated by keeping the spectrometers in a fixed position during all analyses. This precludes the collection of backgrounds during the analysis. However, the background count rates do not vary significantly from one inclusion to another during an analytical session because of the nearly constant major element composition of rhyolitic glass inclusions in quartz. Small variations in the backgrounds are insignificant with respect to the large peak-to-background ratio for the major elements. After the initial calibrations for the elements included in element package 1, a rhyolitic glass inclusion was analyzed and backgrounds were collected for each element. These background count rates were stored in memory for use in subsequent analyses, thus there was no need to move the spectrometers to collect backgrounds during the analyses. The spectrometers were then moved to the peak positions that were determined during the initial calibration, then they remained fixed. A standard calibration was performed again but this time without re-collecting the standard backgrounds that had been determined only a few minutes earlier. This second standard calibration was performed to determine the count rate on the standards at the fixed spectrometer position. By keeping the spectrometers in a fixed position during the major element analytical session (i.e., step 1), analytical uncertainty was limited to the error in counting statistics and beam-current drift. As further discussed below, analytical conditions for element package 1 were typically 20 s counting times with a 30 μm beam diameter at 15 nA specimen current (15 keV acceleration potential).

The loss of Na_2O during exposure to the electron beam was corrected following the method of Nielsen and Sigurdsson (1981) and Jercinovic and Keil (1988). The diameter of the microprobe beam was set at 30 μm unless the glass inclusion was <35 μm in diameter. The beam was set to cover as much of the glass inclusion as possible without overlapping onto the host quartz crystal in the cases in which the glass inclusions were <35 μm. Five separate 20 s analyses (with ZAF matrix corrections) were performed on the same spot of the glass inclusion, and the cup current was measured between each analysis. Counting began immediately upon the sample's exposure to the electron beam, but the sample remained exposed to the beam for 8.1 s after the counting ceased. Thus, the duration of the first analysis was 10 s (i.e., one-half the counting time of the first analysis) and the durations of the remaining four analyses were 38.1, 66.2, 94.3, and 122.4 s. During the analyses, the loss of Na from the volume of glass affected by the electron beam was a function of electron-beam exposure time. The Na abundance in the glass before exposure can be calculated by (1) plotting $\ln(Na_2O)$ against cumulative electron-beam exposure time, (2) fitting a linear regression through the data, and (3) calculating the initial Na abundance at 0 s (Nielsen and Sigurdsson 1981; Jercinovic and Keil 1988).

Although the analytical precision achieved for all elements can be improved using longer counting times and higher specimen currents, under these conditions the Na_2O abundance approaches a minimum value (Fig. 2a). With a certain amount of Na loss, plots of time vs. $\ln(Na_2O)$ become nonlinear (Fig. 2b). The analyses in Figure 2 were performed with excessively long counting times and high beam currents to illustrate that the Na abundance asymptotically approaches a minimum with prolonged exposure to the electron beam. The minimum Na_2O concentration depends on the beam current and the beam diameter and is lower with higher specimen currents and smaller beam diameters. It is important to choose the

TABLE 1. Analytical conditions for typical analyses of rhyolitic glass inclusions in quartz phenocrysts ($K\alpha$ peaks measured)

Element	Spectrometer crystal	Detection limit (wt%)	Calibration standard	Typical abundance (wt%)
SiO_2*	TAP	0.11	kyanite	73.72
TiO_2	PET	0.016	rutile	0.205
Al_2O_3*	PET	0.038	kyanite	11.54
FeO**	LIF	0.010	synthetic fayalite	1.81
MnO	LIF	0.014	tephroite	0.067
MgO	TAP	0.004	synthetic forsterite	0.236
CaO	PET	0.032	diopside	1.84
Na_2O*	TAP	0.044	jadeite	3.04
K_2O*	PET	0.032	orthoclase	2.23
Cl	PET	0.004	sodalite	0.257
Total	—	—		94.94†

Note: Typical results are from analyses performed on a melt inclusion in a quartz phenocryst from the Otsquago Creek bentonite.

* Total of five analyses on the same spot, count time = 20 s per analysis for a total of 100 s at 15 nA cup current in analytical step 1. Counts and backgrounds listed are for the first of the five analyses. Others, cup current = 45 nA, count time = 180 s.

** Total Fe as FeO.

† Difference in sum of oxides from 100 wt% is due to the presence of dissolved volatiles.

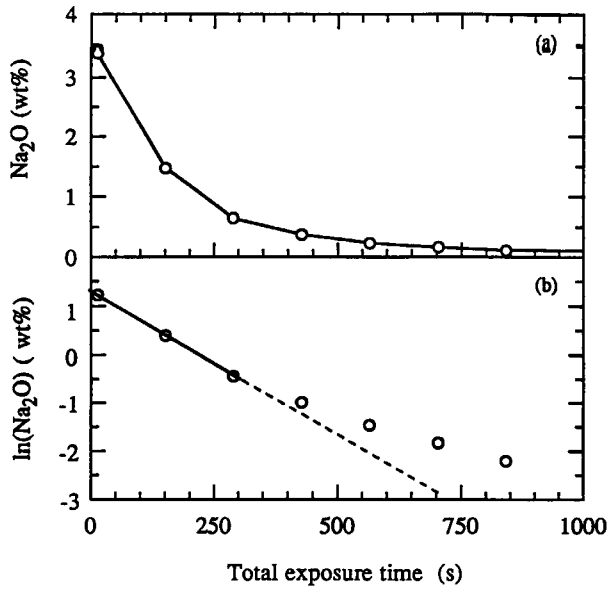

FIGURE 2. (a) Results of replicate Na_2O analyses on the same spot of a rhyolitic glass standard as a function of total electron-beam exposure time. Note the well-known loss of Na_2O during the analysis of a hydrous rhyolitic glass and the approach to a minimum Na_2O concentration at long counting times. (b) Same data plotted as the natural logarithm of the Na_2O concentration as a function of total electron-beam exposure time. Note the deviation from a straight line on this plot making it impossible to extrapolate the data back to 0 s exposure time to obtain the original Na_2O content with the use of the technique of Nielsen and Sigurdsson (1981). Sample analyzed with an accelerating potential of 15 keV and a beam current of 60 nA focused on a spot size of 20 μm. The extraordinarily long counting times and high specimen currents were used to emphasize the approach to a minimum value for Na_2O with increasing exposure time.

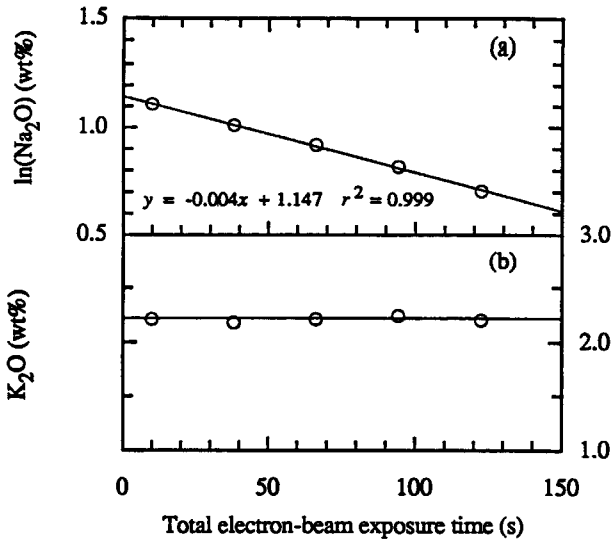

FIGURE 3. (a) Results of replicate analyses of a single spot on a glass inclusion from the Otsquago Creek bentonite. This inclusion was analyzed with an accelerating potential of 15 keV and a beam current of 10 nA focused on a spot size of 20 μm. Note the linear trend of the natural logarithm of Na_2O as a function of total electron-beam exposure time. (b) Results of the analyses shown in a for K_2O. Note that, although Na_2O is mobilized, no K_2O loss or apparent increase in K_2O resulting from Na loss is observed.

counting time, beam current, and beam size that provide sufficiently precise data while remaining on the linear segment of the Na_2O-loss curve. By not collecting backgrounds for each analysis, more analyses can be performed within a given time interval, which ensures that sufficient data are collected for the time regression. We found empirically that a ratio of beam diameter (micrometers) to beam current (nanoamperes) of about two provides optimal conditions for analysis of Na_2O in hydrous rhyolitic glass inclusions. For example, during each 20 s analysis of a 35 μm glass inclusion, a 30 μm beam with a current of 15 nA would be used. Smaller inclusions required 20 s analysis with a smaller beam diameter and a lower current. This means that more precise major element analyses with the use of element package 1 can be achieved on larger glass inclusions. Figure 3a is a plot showing the rate of loss of Na_2O during a typical analysis.

Although K_2O is also mobile under the electron beam (Nielsen and Sigurdsson 1981), we found that under the operating conditions described above, the K concentration remains constant within analytical uncertainty (Fig. 3b). SiO_2 and Al_2O_3 may display slight apparent increases because of the mobilization of Na_2O, but the increases are typically smaller than the uncertainty in the analyses.

Mg, Ti, Al, Cl, and Fe were analyzed in element package 2, with only one element assigned to each spectrometer. To obtain high-precision analyses, long counting times on the peak (200 s) and high specimen currents (40 nA) were used. In addition, 200 s backgrounds were collected during each analysis for each minor and trace element. The background count rate determined for Al_2O_3 (major element) on the first analysis of step 1 was applied to all subsequent Al analyses of the rhyolitic glass inclusions. Consequently, the spectrometer allocated to Al was stationary during all subsequent analyses. When each analysis using element package 2 was complete, the ZAF matrix corrections (calculated using a fixed glass-inclusion composition stored in computer memory) were then applied to the raw data. The effect of dead time for Al counts at these high specimen currents and long counting times (i.e., 45 nA and 200 s) could not be detected. The high specimen current and long counting times used in step 2 caused further decreases in alkali abundances with concomitant increases in the abundances of the conserved, nonmobile elements. Because only one element was analyzed by each spectrometer during the entire analysis, all the elements increased owing to Na loss by the same proportion. This effect can be accommodated by using the simple relationship for Al normalization

$$X_{\text{norm}} = \frac{[Al_2O_3]_{\text{step 1}}}{[Al_2O_3]_{\text{step 2}}} \cdot X_{\text{step 2}} \quad (1)$$

TABLE 2. Results of electron microprobe analyses (wt%) of rhyolitic glass inclusions in quartz phenocrysts from the Otsquago Creek bentonite of Ordovician age

	SiO_2*	TiO_2	Al_2O_3*	FeO**	MnO	MgO	CaO	Na_2O	K_2O*	Cl	Total†
1a‡	73.72(21)	0.205(6)	11.54(5)	1.81(1)	0.067(5)	0.236(3)	1.84(1)	3.04(6)	2.23(3)	0.257(4)	94.94(23)
1b‡	73.95(22)	0.210(6)	11.31(12)	1.78(1)	0.071(5)	0.237(3)	1.79(1)	3.09(6)	2.21(5)	0.251(4)	94.90(26)
2	73.11(27)	0.213(6)	11.63(4)	1.83(1)	0.069(5)	0.250(3)	1.82(1)	3.22(7)	2.23(8)	0.254(4)	94.63(29)
3	72.73(26)	0.217(6)	11.59(5)	1.83(1)	0.061(5)	0.239(3)	1.78(1)	3.13(7)	2.22(4)	0.252(4)	94.04(28)
4	73.25(28)	0.213(6)	11.57(4)	1.85(1)	0.064(5)	0.251(3)	1.90(1)	3.51(7)	2.21(5)	0.256(4)	95.07(29)
5	74.18(21)	0.205(6)	11.38(6)	1.82(1)	0.058(4)	0.242(3)	1.82(1)	3.25(7)	2.26(3)	0.257(4)	95.47(23)
6a‡	73.72(20)	0.215(6)	11.51(11)	1.88(1)	0.074(5)	0.244(3)	1.82(1)	3.15(7)	2.23(5)	0.263(4)	95.10(24)
6b‡	74.15(27)	0.209(6)	11.46(9)	1.84(1)	0.077(6)	0.241(3)	1.80(1)	3.16(7)	2.16(4)	0.251(4)	95.35(29)
6c‡	73.70(14)	0.219(7)	11.52(10)	1.83(1)	0.064(5)	0.242(3)	1.83(1)	3.15(7)	2.25(4)	0.257(4)	95.05(19)
7	73.31(29)	0.210(6)	11.58(6)	1.81(1)	0.068(5)	0.242(3)	1.79(1)	3.24(7)	2.24(7)	0.261(4)	94.74(32)
8a‡	73.42(18)	0.192(6)	11.34(9)	1.82(1)	0.060(4)	0.237(3)	1.79(1)	3.50(7)	2.25(4)	0.249(4)	94.86(22)
8b‡	73.54(26)	0.218(7)	11.32(7)	1.83(1)	0.071(5)	0.241(3)	1.78(1)	3.46(6)	2.26(8)	0.250(4)	94.56(29)
9	72.30(23)	0.207(6)	11.58(6)	1.83(1)	0.067(5)	0.249(3)	1.80(1)	3.46(7)	2.26(4)	0.258(4)	94.01(25)
10	73.12(29)	0.214(6)	11.66(4)	1.83(1)	0.062(5)	0.253(3)	1.79(1)	3.34(7)	2.31(5)	0.269(4)	94.85(30)
11	73.39(28)	0.200(6)	11.43(5)	1.77(1)	0.065(5)	0.236(3)	1.84(1)	3.26(7)	2.21(3)	0.254(4)	94.66(30)
Mean	73.44(51)	0.21(7)	11.49(11)	1.82(3)	0.066(5)	0.243(6)	1.81(3)	3.26(16)	2.24(3)	0.256(5)	94.83(55)

Note: Numbers in parentheses are the analytical uncertainties and are equal to the last decimal place of the measured value.

* Analytical uncertainty is the 1σ uncertainty of five analyses on the same spot. Uncertainty of total was calculated using the equation $\sigma_{total} = (\sigma_a^2 + \sigma_b^2 \ldots)^{0.5}$. All other uncertainties are based on counting statistics (see text).

** Total Fe expressed as FeO.

† Deviation of totals from 100% is due to the presence of volatiles [e.g., H_2O dissolved in these glasses (e.g., Rutherford et al. 1985)].

‡ Sample numbers with letters represent analyses of different inclusions in the same phenocrysts.

where X_{norm} is the Al-normalized abundance of element X, $X_{step\ 2}$ is the abundance of element X measured in step 2, and $[Al_2O_3]_{step\ 1}$ and $[Al_2O_3]_{step\ 2}$ are the abundances of Al_2O_3 measured in steps 1 and 2, respectively. The results of these analyses on glass inclusions from the Otsquago Creek bentonite are shown in Table 2. Following the analyses of all glass inclusions with the use of element package 2, analyses were made of all glass inclusions using element package 3 (Mg, Ca, Al, Mn, Fe). As in the case of packages 1 and 2, each of the five spectrometers was assigned one element only. The operating conditions and Al normalization were identical to those used in step 2.

Table 1 lists the typical values of the detection limits for each element for the operating conditions described above. Note that these methods yield detection limits for most elements that are at least a factor of ten lower than the abundances of the elements in common rhyolitic glass inclusions.

Precision, reproducibility, and accuracy

The precision of the Na_2O data obtained using the technique described above can be assessed by calculating the uncertainty of the value obtained by extrapolating $\ln(Na_2O)$ to 0 s beam-exposure time (i.e., the Y intercept). The measured concentration of Na_2O in 15 glass inclusions from the Otsquago Creek bentonite that were each analyzed five times with 10–15 nA specimen currents, 20 s counting times per analysis, and 20–30 μm beam diameters are listed in Table 2 along with the calculated uncertainties. The uncertainties of the values are approximately 1.5–3.0% of the total Na_2O for these analytical conditions, which is similar to the average 1σ uncertainties for each analysis on the same spot calculated on the basis of counting statistics. The uncertainties in K_2O, Al_2O_3, and SiO_2 are taken as the standard deviation of the five replicate analyses on each inclusion performed in step 1. These agree well with the 1σ uncertainty calculated using counting statistics. The precisions of the analyses of minor and trace elements reported in this study were calculated on the basis of counting statistics.

Note that element packages 2 and 3 involve duplicate analyses for Al, Fe, and Mg. Although the Al-normalization method necessitates that Al be analyzed in all three element packages, duplicate analyses of Mg and Fe allow analytical reproducibility to be evaluated. Figures 4a and 4b demonstrate the high precision that can be achieved by these analytical methods. Figures 4a and 4b show the results of replicate analyses that were obtained over a period of 2 yr for MgO and FeO on 460 glass inclusions from many different bentonitic tephras. If the reproducibility were perfect, these data would form a straight line with a slope of 1 trending through the origin on these plots. The data plotted in Figure 4 clearly demonstrate the high precision and excellent reproducibility of these analyses.

To demonstrate the precision and reproducibility of these analyses from one analytical session to another, three working standards were analyzed using element packages 2 and 3 during each analytical session over a period of eight months. These three working standards are hydrous, rhyolitic glass inclusions from separate, unrelated, compositionally distinct eruptive events (Table 3). The results of 23 analyses on each of the three working standards by two operators are shown in Figure 5. Figure 5 not only demonstrates the analytical precision and reproducibility of these data but also the ability to distinguish unambiguously different rhyolitic glass compositions. The enhanced precision of this technique offers, for the first time, the ability to distinguish minor and trace element

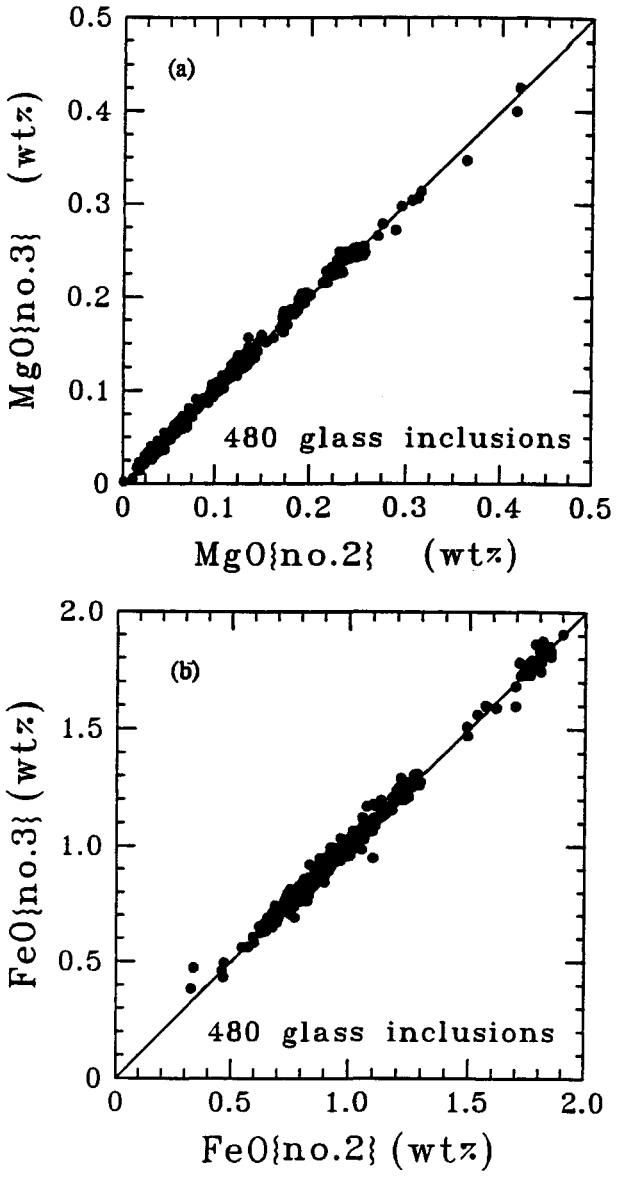

FIGURE 4. Results of replicate analyses of glass inclusions for (a) MgO and (b) FeO. Some of the analyses were performed on different days with different machine calibrations. Perfect reproducibility would be a straight line trending through the origin with a slope of 1 on this diagram.

compositional differences among glass inclusions from single bentonitic tephras and the recognition of chemical trends in populations of glass inclusions from these layers (Fig. 5). Distinguishing chemical trends of minor and trace elements not only provides important geochemical information that would not be discernible using lower precision electron microprobe methods, but the chemical trends provide yet another chemical fingerprint of the bentonitic tephras. For example, the plus signs in Figure 5 are the results of electron microprobe analyses of glass inclusions in different phenocrysts from a single bentonitic tephra

TABLE 3. Composition (wt%) of the three glass inclusions used as working standards

	1	2	3
SiO_2	73.21	73.11	75.16
TiO_2	0.221	0.047	0.118
Al_2O_3	11.63	11.84	11.89
FeO*	1.82	0.81	1.25
MnO	0.067	0.062	0.033
MgO	0.247	0.049	0.030
CaO	1.88	0.66	0.67
Na_2O	3.60	3.51	2.82
K_2O	2.22	4.76	5.01
Cl	0.270	0.131	0.019
Total	95.16	94.97	97.06

Note: 1 = melt inclusion in quartz from the Otsquago Creek bentonite, 2 = melt inclusion in quartz from the Youngest Toba Tuff (YTT), and 3 = melt inclusion in quartz from a bentonite in the Lower Devonian Esopus Formation at Cherry Valley, New York. Note the compositional variability among the glasses.
* Total Fe as FeO.

from the Mandata Formation (Lower Devonian) from the Central Appalachian Basin. The enhanced precision of the analyses distinguishes a strong covariation between MgO and FeO. A bimodal distribution of CaO and possibly TiO_2 can also be discerned. Both of these chemical characteristics serve as excellent chemical fingerprints of this particular bentonitic tephra layer that can be distinguished only by using this high-precision electron microprobe technique.

The accuracy of our analyses were evaluated by analyzing a set of well-characterized rhyolitic glass standards, the compositions of which are presented in Devine et al. (1995). The results of the analyses of these glasses are presented in Table 4 and are in excellent agreement the values stated in Devine et al. (1995).

Volatiles

The dissolved volatiles in rhyolitic glass inclusions have been measured by several techniques and have been found to be primarily H_2O with lower abundances of CO_2 (e.g., Stolper 1982; Karsten et al. 1982; Sommer and Schramm 1983; Anderson et al. 1989; Hervig et al. 1989; Dunbar et al. 1989; Newman et al. 1986, 1988; Dunbar and Hervig 1992a, 1992b; Bacon et al. 1992; Devine et al. 1995). A simple method for estimating total volatile content dissolved in glasses is by subtracting the oxide totals from 100 wt% (e.g., Anderson 1973, 1974; Beddoe-Stephens et al. 1983; Rutherford et al. 1985; Sommer 1977; Devine et al. 1995). The assumption is that the difference between the sum of all the major, minor, and trace element oxides and 100 wt% corresponds to the chemical species that are not measured with the electron microprobe, which consist primarily of H_2O. The small concentrations of unmeasured elements and CO_2 are considered negligible. The total volatile content determined by this technique for the inclusions from the Otsquago Creek bentonite range from 4.5 to 6.0 wt% (Table 2). The uncertainties in the volatile abundances estimated by this technique are principally dependent upon the accuracy of the analytical techniques for the major elements Si and Al. The quality

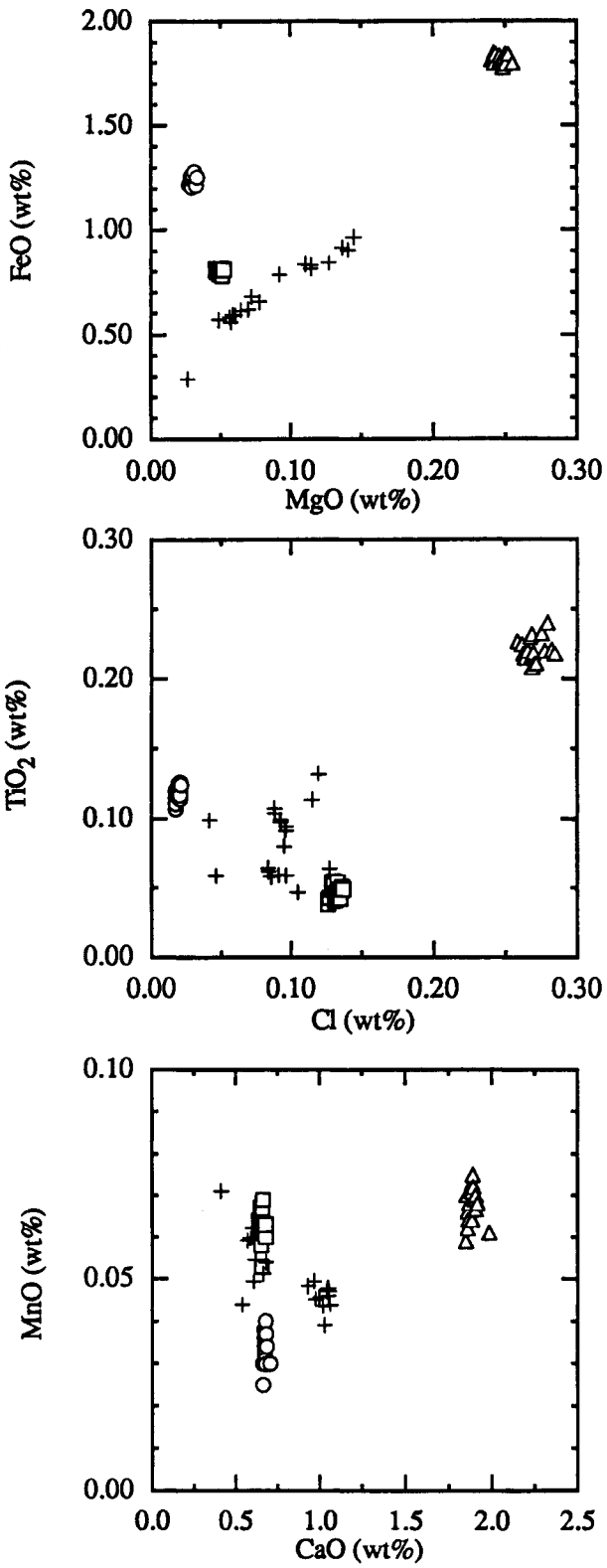

FIGURE 5. Results of replicate analyses performed on three glass inclusions that were used as working standards from one analysis session to another. Plot shows 23 separate analyses of the three working standards (Table 3) collected over a period of eight months by two operators. The circles are data for a glass inclusion from the Esopus Formation at Cherry Valley, New York. The squares are data for a glass inclusion from the Toba Tuff. The triangles are the results for a glass inclusion from Otsquago Creek bentonite. The plus signs are the results of analyses of different glass inclusions from a single bentonitic tephra from the Devonian Mandata Formation in the Central Appalachian Basin. Note the strong covariation between MgO and FeO and the bimodal distribution of CaO among this population of inclusions. This detail would not be detectable using lower precision electron microprobe techniques.

→

of data obtained by the analytical methods described above permits the volatile content of the rhyolitic glass inclusions to be estimated with reasonable accuracy and precision. By propagating the uncertainties for each oxide through the sum calculation, uncertainties were calculated ranging from 0.18 to 0.32 wt% (Tables 2 and 4). This estimated 1σ uncertainty for the oxide totals ($\pm$0.2–0.3 wt%) corresponds to the uncertainties in the volatile contents obtained using the difference-in-sum method, which is similar to the precision obtained by ion microprobe (Devine et al. 1995).

Estimates of the volatile contents of the hydrous standard glasses are listed in Table 4 along with the H_2O content measured by Devine et al. (1995) using Fourier-transform infrared spectroscopy (FTIR). The H_2O contents measured by FTIR are systematically lower than the estimates calculated by difference, consistent with the results of Devine et al. (1995). This discrepancy cannot be explained by the presence of Fe^{3+}. Although the experiments were performed under relatively oxidizing conditions ($\log f_{O_2}$ = NNO + 1), the molar Fe_2O_3/FeO ratio calculated from the equation of Kilinc et al. (1983) is approximately 0.16. Thus, the reason for the systematic differences among the volatile values measured by FTIR and those estimated by difference is unclear at this time.

Although the analytical methods for the electron microprobe described here provide high-quality data, there is a "down-side" to this general approach. Instead of the large number of analyses that most electron microprobe operators are familiar with (e.g., 100 major element analyses per 10 h session), the methods described here yield complete analyses (element packages 1, 2, and 3) for only about 12–15 glass inclusions in a 10 h session. The compromise is a classic one: quantity vs. quality.

INSTRUMENTAL NEUTRON ACTIVATION ANALYSES (INAA)

Analytical technique

Quartz crystals selected for INAA were free of optically visible mineral inclusions and fractures. The crystals were soaked in 28.9 *N* hydrofluoric acid at room temperature

TABLE 4. Electron microprobe analyses of H_2O-bearing glasses from Devine et al. (1995)

Sample	494	495	498	508	510
SiO_2	73.35(13)	75.49(13)	72.97(13)	74.35(13)	70.95(13)
TiO_2	0.070(6)	0.076(6)	0.077(6)	0.081(6)	0.075(6)
Al_2O_3	12.06(3)	12.38(3)	12.00(3)	12.25(3)	11.66(3)
FeO*	0.99(1)	1.03(1)	0.69(1)	1.00(1)	0.95(1)
MnO	0.052(5)	0.053(5)	0.048(5)	0.058(5)	0.052(5)
MgO	0.046(2)	0.044(2)	0.047(2)	0.045(2)	0.045(2)
CaO	0.350(6)	0.342(6)	0.354(6)	0.342(6)	0.346(6)
Na_2O	4.18(2)	4.32(3)	4.20(5)	4.27(4)	4.15(3)
K_2O	4.50(7)	4.64(7)	4.49(7)	4.57(7)	4.31(6)
Cl	0.104(3)	0.112(3)	0.097(3)	0.099(3)	0.089(3)
Total**	95.71(18)	98.49(18)	95.05(18)	97.18(18)	92.74(18)
H_2O (FeO)†	4.30(18)	1.61(18)	5.03(18)	2.93(18)	7.37(18)
H_2O by FTIR‡	4.09(4)	1.42(3)	4.72(10)	2.58(2)	6.23(9)

Note: Numbers in parentheses are the analytical uncertainties (1σ) and are equal to the last decimal place of the stated value.
* Total Fe expressed as FeO.
** Uncertainty in total calculated using method described in Table 2.
† H_2O content calculated by difference using the data shown above, assuming all Fe is FeO.
‡ H_2O measured by Fourier-transform infrared spectroscopy (FTIR) from Devine et al. (1995).

for approximately 30 min, washed in water, and then placed in immersion oil for microscopic examination. The initial soaking highlighted cracks in some crystals that had not been visible prior to HF treatment. Crystals displaying these cracks were broken along the cracks and soaked again in hydrofluoric acid to remove any material adhering to the crack surfaces. The crystals were then soaked in hot (about 100 °C) 12 *N* hydrochloric acid for 3 h to remove surface contamination from handling of the grains with stainless steel tweezers, rinsed in distilled water, and placed in prewashed glass vials for shipment from SUNY, Albany, to NASA, Houston. Upon arrival at Johnson Space Center, the samples were individually weighed to a precision of ± 2 μg and sealed in high-purity silica glass tubes along with well-characterized glass standards (Lindstrom 1990). The samples and standards were irradiated for 160 h in the core of the Missouri University Research Reactor, Columbia, Missouri, at a neutron flux of 6.2×10^{14} n/(cm^2·s). After irradiation, all samples and standards were individually repackaged in plastic sandwich assemblies for Ge γ-ray detectors with efficiencies of 55 and 59% (at 1332 keV, relative to 3 × 3 in. NaI). These detectors were surrounded by walls made from low-background materials (1 m thick walls filled with crushed

TABLE 5. Typical results of instrumental neutron activation analyses

Sample	OC-22	OC-24	OC-6	OC-23	Avg. inclusion-free quartz
Mass (μg)	133.4	38.7	32.3	98.9	
Na_2O (wt%)	0.1679(24)	0.0925(13)	0.0317(5)	0.0074(1)	0.00042(7)
K_2O (wt%)	0.121(8)	0.072(4)	0.0248(9)	0.0058(5)	<0.00021
FeO (wt%)*	0.0916(12)	0.0543(9)	0.0204(4)	0.0065(1)	0.0026(6)
Sc	0.532(6)	0.313(4)	0.1118(14)	0.0300(4)	0.0028(3)
Co	0.088(3)	0.053(4)	0.0205(19)	0.0088(6)	0.008(5)
Rb	3.55(11)	2.09(13)	0.74(7)	0.17(2)	<0.0246
Cs	0.143(6)	0.084(7)	0.028(3)	0.007(1)	<0.00092
Sr	5.1(8)	2.7(11)	<1.6	<0.6	<0.396
Ba	27.1(10)	16.3(12)	5.6(6)	1.3(1)	<0.244
La	1.195(17)	0.707(18)	0.242(8)	0.057(1)	0.0020(4)
Ce	2.52(4)	1.44(3)	0.477(16)	0.115(4)	0.0044(6)
Sm	0.252(3)	0.1426(28)	0.0523(11)	0.0126(2)	0.0006(3)
Eu	0.039(4)	0.023(4)	0.0065(18)	0.0019(5)	0.00050(22)
Tb	0.0392(11)	0.0228(13)	0.0079(6)	0.0018(2)	<0.00039
Yb	0.178(4)	0.108(5)	0.0357(29)	0.0084(5)	0.00028(13)
Lu	0.0275(9)	0.0162(1)	0.0058(5)	0.0014(1)	<0.00010
Zr	7.9(14)	<8	2(1)	<1	<0.17
Hf	0.201(6)	0.115(6)	0.0408(27)	0.0103(7)	0.00082(51)
Ta	0.0302(25)	0.017(4)	0.0065(25)	0.002(4)	<0.0007
U	0.132(5)	0.077(9)	0.026(5)	0.007(1)	<0.00065
Th	0.36(6)	0.220(5)	0.0765(23)	0.0172(6)	<0.00069
As	0.424(21)	0.286(24)	0.094(9)	0.025(3)	0.0011(6)
Sb	0.0267(2)	0.0177(27)	0.0066(14)	0.0015(4)	0.00077(42)
Zn	2.8(1)	1.53(16)	0.59(8)	0.275(25)	0.20(2)
Br	0.34(6)	0.2(1)	0.061(24)	0.013(7)	0.0039(13)

Note: Average concentrations of elements in four crystals with no glass inclusions are also included. Abundances are in parts per million, except where otherwise noted. Numbers in parentheses are the analytical uncertainties (1σ) and are equal to the last decimal place of the measured value. Numbers preceded by "<" are 2σ upper limits.
* Total Fe expressed as FeO.

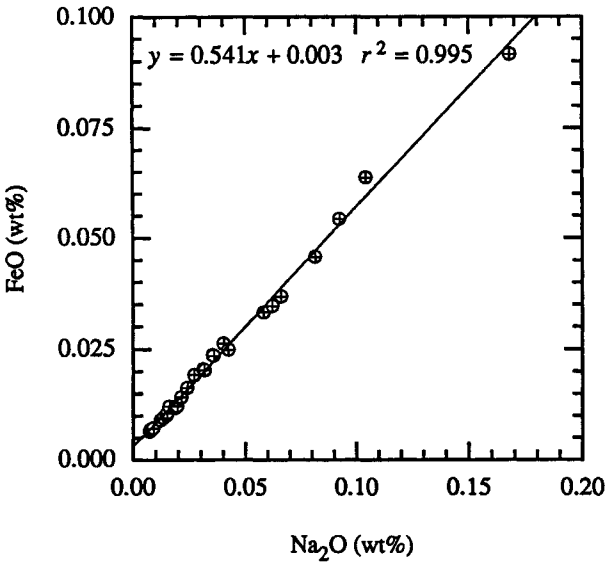

FIGURE 6. Results of INAA analyses of glass inclusions in quartz phenocrysts from the Otsquago Creek bentonite. These data are in raw form, and the plot shows that the trend of this line does not pass through the origin as would be expected if the host quartz was pure SiO_2.

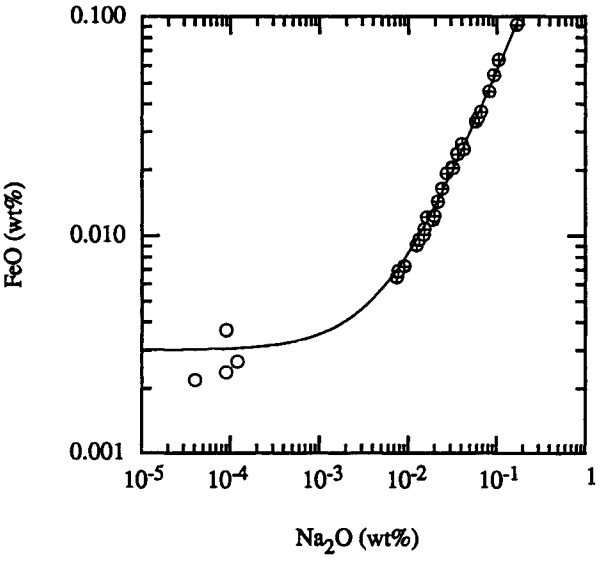

FIGURE 7. Results of INAA analyses of glass inclusions in quartz phenocrysts from the Otsquago Creek bentonite (circles with plus signs). The plot is the same as in Figure 6 but is on a log scale and the data from inclusion-free quartz crystals are included (open circles). Note that the extension of the linear regression passes through the inclusion-free quartz data set.

dunite), and the detectors were situated in 10 cm thick lead shields lined with cadmium and copper foil to reduce backgrounds from cosmic rays. Because the radioactive decay of radon gas is a significant source of background γ-ray peaks, the air inside the lead shields was displaced by plastic boxes filled with nitrogen to decrease the amount of radon gas in the proximity of the detectors. Backgrounds were collected after every set of analyses by counting for several hours with no sample on the detector. Sources of background counts include radioactive decay of radon gas, cosmic $\beta+$ annihilation, and environmental ^{40}K emissions.

Samples were counted three times for a total of about 48 h. Spectral data were reduced using a set of interactive modular programs called Trace Element Analyses By Automated Gamma-ray Spectrometry (TEABAGS), described in Lindstrom and Korotev (1982). Lindstrom (1990) estimated that, by using this high neutron fluence, the low-background facility, and the enhanced sample geometry, the sensitivity of the analyses would increase by a combined factor of approximately 30000 times over that of normal INAA. This technique, which has been successful in measuring the trace element concentrations in cosmic dust particles with masses as small as tens of nanograms (Lindstrom 1990), was applied in the current study to determine the trace element compositions of rhyolitic glass inclusions in quartz phenocrysts.

Calculation and normalization procedures

Four representative analyses (out of 27 performed) of glass-inclusion–bearing quartz phenocrysts from the Otsquago Creek bentonite layer are presented in Table 5. Because the entire crystal was irradiated, these data represent the abundances of elements in the entire grain (i.e., the rhyolitic glass inclusion plus the quartz host). Most elements have quartz-glass partition coefficients $\ll 1$ under magmatic conditions; therefore, most of the measured elements reside in the glass inclusions. The quartz host behaves as a dilutant. This was confirmed by analyzing euhedral to subhedral quartz crystals devoid of glass inclusions from the same bentonitic tephra layer (Table 5). These inclusion-free crystals provided the concentrations of all elements in the quartz phenocrysts alone, which are present at less than the parts per million level in most cases (Table 5).

Figure 6 is a plot of FeO vs. Na_2O (for 27 quartz phenocrysts with glass inclusions) and shows that the measured abundances fall on a straight line trending toward the origin. If the host quartz crystals were pure SiO_2, the data should intersect the origin. Quartz crystals having the largest mass fraction of rhyolitic glass to quartz would plot farthest from the origin. Consequently, this is a two-component mixing line between quartz and the rhyolitic glass. Figure 7 is similar to Figure 6, except that a logarithmic scale is used and the inclusion-free quartz data are included. Note that the extension of the linear regression passes through the inclusion-free quartz data. The line is curved in log-log space because there is a nonzero Y intercept. The contribution to the measured elemental abundances by the quartz host can be corrected by subtracting the inclusion-free abundances from the raw data. For some elements, the concentration of the contaminants in the host quartz crystals can be measured by INAA

TABLE 6. Equations of regression lines through each element plotted against Na_2O (host corrected) as measured by INAA

Element	Y intercept	Regression coef. (r^2)
K_2O (wt%)	0.0015%	0.997
FeO (wt%)	0.0032%	0.997
Sc	0.0083	0.998
Co	0.0074	0.929
Rb	0.0280	0.995
Cs	0.0017	0.997
Sr	0.6760	0.865
Ba	0.3352	0.994
La	0.0114	0.998
Ce	0.0155	0.998
Sm	0.0023	0.998
Eu	0.0005	0.987
Tb	0.0004	0.997
Yb	0.0016	0.997
Lu	0.0003	0.997
Zr	0.9615	0.862
Hf	0.0027	0.998
Ta	0.0005	0.995
U	0.0012	0.990
Th	0.0039	0.996
As	0.0092	0.993
Sb	0.0008	0.897
W	0.0203	0.493
Zn	0.0203	0.997
Br	0.0148	0.977

Note: All data in parts per million, except where otherwise noted.

TABLE 7. Ratios of trace elements

Sc/Ce	Th/As	Ba/Hf	Sc/Hf	Cs/Ce	Sc/Th
0.22(3)	0.80(12)	139(15)	2.6(7)	17(3)	1.59(29)
0.22(3)	0.76(10)	139(15)	2.7(6)	16(3)	1.48(25)
0.23(3)	0.77(9)	138(11)	2.7(6)	17(3)	1.49(23)
0.22(3)	0.79(10)	147(19)	2.7(7)	18(3)	1.48(26)
0.23(3)	0.81(8)	137(17)	2.7(7)	17(3)	1.46(25)
0.22(3)	0.76(10)	138(15)	2.7(7)	16(3)	1.52(26)
0.24(3)	0.78(13)	123(19)	2.7(7)	17(3)	1.60(30)
0.22(4)	0.86(17)	141(24)	2.6(7)	18(4)	1.54(29)
0.22(3)	0.74(6)	131(11)	2.7(6)	16(3)	1.49(23)
0.23(3)	0.82(13)	149(17)	2.9(7)	18(3)	1.55(27)
0.23(4)	0.83(9)	138(20)	2.7(8)	16(4)	1.47(29)
0.23(4)	0.72(13)	160(25)	2.9(8)	17(4)	1.58(30)
0.22(4)	0.81(11)	121(18)	2.8(8)	18(4)	1.47(28)
0.23(4)	0.67(10)	132(29)	2.8(8)	19(4)	1.6(3)
0.22(2)	0.83(7)	153(11)	2.8(6)	18(3)	1.45(22)
0.22(3)	0.80(8)	135(11)	2.7(6)	17(3)	1.46(23)
0.23(4)	0.79(12)	120(17)	2.6(7)	16(3)	1.52(27)
0.21(2)	0.85(4)	135(6)	2.7(5)	18(2)	1.48(19)
0.26(4)	0.69(9)	129(16)	2.9(8)	16(3)	1.7(3)
0.22(2)	0.77(7)	142(13)	2.7(6)	17(3)	1.42(21)
0.21(3)	0.70(8)	132(13)	2.7(6)	16(3)	1.51(25)
0.22(2)	0.81(4)	139(7)	2.8(5)	16(2)	1.49(20)
0.22(2)	0.78(3)	143(9)	2.8(6)	18(3)	1.51(23)
0.22(3)	0.74(7)	128(11)	2.7(6)	18(3)	1.56(24)
0.22(2)	0.76(5)	145(10)	2.7(5)	18(3)	1.48(22)
0.23(2)	0.77(4)	132(9)	2.7(5)	17(2)	1.55(22)
0.22(3)	**0.78(5)**	**137(9)**	**2.7(1)**	**17.0(8)**	**1.52(7)**

Note: Numbers in bold in the last row are the mean and standard deviations of the values in the corresponding columns. Numbers in parentheses are the analytical uncertainties (1σ) and are equal to the last decimal place of the measured value.

(e.g., FeO = 26 ± 6 ppm: Table 5). However, the INAA technique is not sensitive enough to obtain sufficiently precise concentrations of other elements (e.g., K, Rb, Cs, Ba) in the inclusion-free quartz crystals. For this reason, the inclusion-free data for all elements (except Na_2O) were calculated as follows. The average concentration of Na_2O in the four analyzed inclusion-free crystals was subtracted from the Na_2O concentration in each of the glass-inclusion–bearing phenocrysts to obtain host-corrected values for Na_2O. The host-corrected Na_2O values were then plotted vs. each element analyzed using Na_2O as the ordinate. The value at which the calculated curve intercepts the abscissa was then taken as the concentration of that element in the quartz host and subtracted from the concentration of that element in each of the glass-inclusion–bearing phenocrysts (regression equations are presented in Table 6). Because the samples are >95% (by mass) quartz, the host-corrected values were simply subtracted from the measured abundances and the quartz component and were not weighted by their mass fractions.

Two important assumptions were made in determining the concentrations of elements in the host crystals with the use of this method: (1) All the glass inclusions are identical in composition; and (2) all the host quartz phenocrysts have identical compositions.

The validity of the first assumption can be addressed by verifying the constancy of ratios among geochemically different elements. Elements that display different partitioning behaviors in igneous systems are compiled in Table 7. These specific elements (Table 7) were chosen because they can be analyzed with high precision by INAA. Because the standard deviations of the elemental ratios are less than or equal to the analytical uncertainties, the variations in glass composition are small relative to the analytical precision of the INAA technique. This is also consistent with electron microprobe analyses of nearly 100 glass inclusions from the Otsquago Creek bentonite and its equivalent at other outcrops that display little or no compositional variation (e.g., Table 2).

The second assumption is more difficult to evaluate. Because the concentrations of impurities in the quartz phenocrysts may vary, it is not possible to determine a unique value for each glass-inclusion–bearing phenocryst. For most elements, the concentrations of elements in the host quartz calculated using the *Y* intercept are within the range of data obtained by INAA for the four analyzed inclusion-free crystals (e.g., Fig. 7). When the *Y* intercept values are used as the host correction for K_2O, the K_2O/Na_2O ratios inferred for the rhyolitic glasses are within the range determined independently by electron microprobe (Table 2). In contrast, when the measured concentrations in the host quartz are used, the K_2O/Na_2O ratios are greater than the range determined by electron microprobe. This suggests that the concentrations in the host quartz derived from the *Y* intercepts are more reliable. The reason for this discrepancy is unclear, but it appears that the compositions of inclusion-free quartz and inclusion-bearing quartz are different for some elements (e.g., Sc, Cs, Rb, Sr). In any case, the *Y*-intercept values

TABLE 8. Typical results of normalizing raw INAA data to the value of Na_2O determined by electron microprobe

Sample	OC-22	OC-24	OC-6	OC-23	Avg. of 27 crystals*
Na_2O (wt%)	3.40(11)	3.23(11)	3.26(12)	3.86(15)	3.41(26)
K_2O (wt%)	2.38(20)	2.35(19)	2.45(16)	2.00(26)%	2.35(21)
FeO** (wt%)	1.76(9)	1.84(10)	1.81(12)	1.48(16)	1.74(15)
Sc	10.4(5)	11.0(6)	10.9(6)	9.8(7)	10.3(8)
Co	1.60(11)	1.65(17)	1.38(23)	0.6(3)	1.6(4)
Rb	70(4)	75(6)	75(8)	62(9)	69(5)
Cs	2.81(19)	2.97(29)	2.8(4)	2.4(4)	2.8(3)
Sr	94(17)	83(40)	<127	<92	<115
Ba	530(3)	580(52)	560(70)	450(70)	530(60)
La	23.5(12)	25.1(14)	24.3(15)	20.5(14)	23.4(17)
Ce	49.8(26)	51.4(28)	48.6(30)	45.0(30)	49.4(30)
Sm	4.97(26)	5.07(27)	5.27(30)	4.70(30)	4.91(30)
Eu	0.77(9)	0.81(15)	0.64(19)	0.66(23)	0.76(13)
Tb	0.77(4)	0.81(6)	0.80(8)	0.67(9)	0.76(6)
Yb	3.51(19)	3.84(26)	3.6(4)	3.09(3)	3.5(3)
Lu	0.54(3)	0.57(5)	0.58(6)	0.48(6)	0.53(4)
Zr	150(29)	<275	171(100)	<281	<223
Hf	3.95(23)	4.06(30)	4.0(4)	3.5(4)	3.85(29)
Ta	0.59(6)	0.60(15)	0.63(27)	0.69(19)	0.58(8)
U	2.60(16)	2.7(4)	2.6(5)	2.5(4)	2.8(4)
Th	7.1(4)	7.8(4)	7.7(5)	6.0(5)	7.1(6)
As	8.3(6)	10.0(10)	8.9(11)	7.2(15)	8.4(10)
Sb	0.51(5)	0.6(1)	0.61(15)	0.30(18)	0.55(18)
Zn	52(4)	49(6)	43(9)	42(13)	51(7)
Br	6.5(12)	6.7(26)	4.9(25)	4(3)	6.5(28)

Note: Values for Na_2O calculated by normalizing data to the value for FeO. All data in parts per million, except where otherwise noted. Numbers in parentheses are the analytical uncertainties (1σ) and are equal to the last decimal place of the measured value. Values preceded by "<" are 2σ upper limits.

* Uncertainty in average of 27 crystals taken as the mean of all data.

** Total Fe expressed as FeO.

provide estimates that are consistent with electron microprobe analyses of glass inclusions in quartz phenocrysts from this layer.

Ni and W abundances were below detection limits and were omitted from the data set. The Cr content of the inclusion-free crystals was surprisingly high, varying from approximately 2 to 25 ppm. The data plotted vs. Na_2O do not form a straight line as expected if the quartz host behaved simply as a dilutant. The reason for the anomalous Cr concentrations is unclear, and Cr has therefore been omitted from the data set.

Because some elements can be analyzed precisely and accurately by both INAA and electron microprobe it is a simple matter to derive the concentration of an element in the glass inclusion by normalizing to an element of known concentration in the glass from electron microprobe analyses,

$$[X]_{\text{glass}} = \frac{[E]_{\text{glass}}}{[E]_{\text{crystal}}} \cdot [X]_{\text{crystal}} \quad (2)$$

where $[X]_{\text{glass}}$ is the calculated concentration of element X in the glass inclusion, $[X]_{\text{crystal}}$ is the host-corrected concentration of element X in the inclusion-bearing quartz crystal measured by INAA, $[E]_{\text{glass}}$ is the known concentration of element E in the glass inclusion as measured by electron microprobe, and $[E]_{\text{crystal}}$ is the host-corrected concentration of element E in the inclusion-bearing quartz crystal measured by INAA. The ratio $[E]_{\text{glass}}/[E]_{\text{crystal}}$ is a measure of the mass fraction of glass inclusion to total crystal. Because the Na_2O and FeO abundances can be precisely and accurately determined by both electron microprobe and INAA, the concentrations of these elements were used to determine the abundance of all other elements obtained by INAA for each grain. The glass compositions derived from Na_2O and FeO normalization are provided in Tables 8 and 9, respectively.

The results of electron microprobe analyses performed on inclusions from the Otsquago Creek bentonite for FeO, MgO, TiO_2, Al_2O_3, Cl, Na_2O, and K_2O are presented in Table 2. Although the concentration of Na_2O varies among glass inclusions (3.0–3.5 wt%) from the same layer, the variation in Na_2O for the Otsquago Creek bentonite is sufficiently small (15%) so as not to affect severely the trace element abundances listed in Tables 8 and 9. For bentonitic tephras that contain populations of glass inclusions of variable composition, each glass inclusion must be analyzed separately by electron microprobe after INAA to obtain a value for the normalizing element. Thus, it is possible to measure the compositions of glass inclusions in different crystals if there is compositional variation among glass inclusions from the same bentonitic tephra. This, however, necessitates reliance on the INAA of inclusion-free quartz crystals as the host correction instead of the Y-intercept method, reducing the accuracy of the host-corrected data.

The analytical uncertainty of the normalized data is calculated by propagating (1) the uncertainty of the INAA, (2) the uncertainty of the electron microprobe analyses (standard deviation of the analyses shown in Table 2), and (3) the uncertainty in the measurements of inclusion-

TABLE 9. Typical results of normalizing INAA data to the value of FeO determined by electron microprobe

Sample	OC-22	OC-24	OC-6	OC-23	Avg. of 27 crystals*
Na_2O (wt%)	3.40(11)	3.23(11)	3.26(12)	3.86(15)	3.41(26)
K_2O (wt%)	2.42(18)	2.48(16)	2.44(13)	2.41(30)	2.44(10)
FeO** (wt%)	1.76(9)	1.84(10)	1.81(12)	1.48(16)	1.74(15)
Sc	10.6(3)	10.7(4)	10.8(4)	12.0(6)	10.7(4)
Co	1.63(8)	1.60(15)	1.37(21)	0.8(4)	1.6(4)
Rb	71(3)	72(5)	74(8)	76(10)	72(4)
Cs	2.87(15)	2.89(26)	2.8(3)	3.0(5)	2.89(15)
Sr	95(17)	81(39)	<125	<113	115(87)
Ba	540(30)	560(46)	550(66)	552(81)	549(35)
La	24(1)	24(1)	24(1)	25.2(13)	24.2(10)
Ce	50(2)	50(2)	48(2)	55(3)	51(2)
Sm	5.06(16)	4.92(19)	5.22(21)	5.76(26)	5.09(30)
Eu	0.78(8)	0.79(14)	0.63(19)	0.80(28)	0.78(11)
Tb	0.79(3)	0.79(5)	0.79(7)	0.83(10)	0.79(5)
Yb	3.58(13)	3.73(21)	3.6(3)	3.8(3)	3.58(18)
Lu	0.55(2)	0.56(4)	0.57(6)	0.59(7)	0.55(3)
Zr	150(30)	<267	170(100)	<344	230(100)
Hf	4.02(17)	3.94(25)	4.0(3)	4.2(4)	3.99(18)
Ta	0.60(5)	0.58(14)	0.63(26)	0.84(22)	0.61(9)
U	2.65(13)	2.7(3)	2.6(5)	3.0(5)	3.0(11)
Th	7.22(25)	7.6(3)	7.6(4)	7.4(5)	7.3(3)
As	8.4(5)	9(1)	9(1)	9(2)	9(1)
Sb	0.52(4)	0.59(10)	0.60(15)	0.37(22)	0.57(18)
Zn	53(3)	47(6)	43(9)	52(15)	53(9)
Br	7(1)	7(3)	5(3)	7(4)	7(3)

Note: Values for FeO calculated by normalizing data to the value for Na_2O. Values for Na_2O calculated by normalizing data to the value for FeO. All data in parts per million, except where otherwise noted. Numbers in parentheses are the analytical uncertainties (1σ) and are equal to the last decimal place of the measured value. Values preceded by "<" are 2σ upper limits.

* Uncertainty in average of 27 crystals taken as the mean of all data.

** Total Fe expressed as FeO.

free quartz crystals through the calculations. Because the uncertainty of the normalizing elements is taken as the standard deviation of the electron microprobe analyses, the heterogeneity of the FeO and Na_2O concentrations among different inclusions from the same bentonitic tephra is accounted for in the final uncertainty.

Equation 2 was used to calculate the total concentration of the elements with the use of both FeO and Na_2O as the normalizing elements. Comparison of the results demonstrates that using either FeO or Na_2O as the normalizing element yields identical results within calculated uncertainty. For example, the average concentration of La in all the inclusions calculated using Na_2O as the normalizing element is 23.4 ± 1.7 ppm, and the average concentration of La calculated using FeO as the normalizing element is 24.2 ± 1.0 ppm.

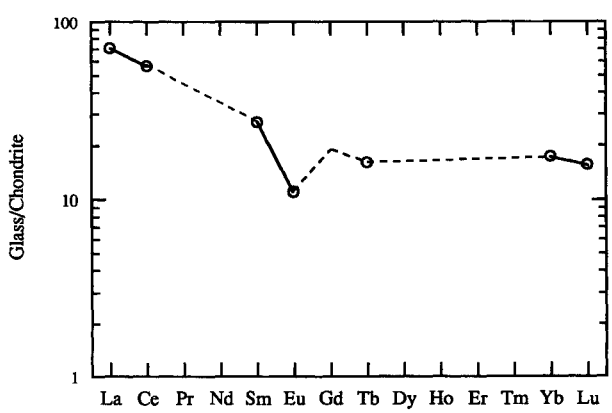

FIGURE 8. Chondrite-normalized REE pattern for the average of all the glass inclusions from the Otsquago Creek bentonite. Note the LREE enrichment and the relatively minor depletion of Eu relative to the other REEs. The dashed lines are extrapolated between elements not analyzed by INAA.

To constrain the accuracy and the internal consistency of the normalized data, the INAA data were compared with the values obtained by electron microprobe analyses for Na_2O, K_2O, and FeO. The average concentration of Na_2O obtained by electron microprobe (3.26 ± 0.16 wt%: mean of the data in Table 2) and the average concentration measured by INAA (3.41 ± 0.26 wt%: normalized to FeO) agree within analytical uncertainty. The average concentration of K_2O obtained by electron microprobe (2.24 ± 0.03 wt%: mean of the data in Table 2) and the average concentration measured by INAA (2.44 ± 0.10 wt%: normalized to FeO) agree within uncertainty. Furthermore, the average concentration of K_2O measured by INAA (2.35 ± 0.21 wt%: normalized to Na_2O) is in agreement with the other two values. The average concentration of FeO obtained by electron microprobe (1.82 ± 0.03 wt%: mean of the data in Table 2) also agrees well with the average concentration measured by INAA (1.74 ± 0.15 wt%: normalized to Na_2O). The INAA and electron microprobe values are identical within analytical uncertainty for all three elements.

Figure 8 is a chondrite-normalized REE pattern of the average glass inclusion from the Ordovician-age Otsqua-

go Creek bentonite. This pattern is typical of the patterns displayed by glasses from rhyodacitic eruptives from the northwestern U.S. (e.g., Izett 1981). The smoothness of the REE pattern (Fig. 8) further demonstrates that the INAA data for these glass inclusions have precision comparable to that of analyses performed on larger glass separates.

Conclusions

The INAA data presented in Tables 8 and 9 represent a suite of elements that have never before been obtained for rhyolitic glass inclusions in quartz. Further analyses using this technique will add to our knowledge of the trace-element compositions of glass inclusions in quartz phenocrysts from other rhyolitic eruptives.

Acknowledgments

The authors wish to thank James F. Luhr, Jeff Grossman, John T. Haynes, and Joseph Devine, whose helpful reviews greatly improved this manuscript. The comments of Glenn Gaetani are also gratefully acknowledged. We thank J. Devine for promptly providing the experimentally produced glass standards. This research was supported by NSF grant EAR-9204931 to J.W.D.

References cited

Anderson, A.T. (1973) The before-eruption water content of some high-alumina magmas. Bulletin Volcanologique, 37, 530–552.

——— (1974) Chlorine, sulfur, and water in magmas and oceans. Geological Society of America Bulletin, 85, 1485–1492.

Anderson, A.T., Newman, S., Williams, S.N., Druitt, T.H., Skirius, C., and Stolper, E. (1989) H_2O, CO_2, Cl, and gas in plinian and ash-flow Bishop Rhyolite. Geology, 17, 222–225.

Bacon, C.R., Newman, S., and Stolper, E. (1992) Water, CO_2, and F in melt inclusions in phenocrysts from three Holocene explosive eruptions, Crater Lake, Oregon. American Mineralogist, 77, 1021–1030.

Beddoe-Stephens, B., Aspden, J.A., and Shepherd, T.J. (1983) Glass inclusions and melt compositions of the Toba Tuffs, northern Sumatra. Contributions to Mineralogy and Petrology, 83, 278–287.

Delano, J.W., Tice, S.J., Mitchell, C.E., and Goldman, D. (1994) Rhyolitic glass in Ordovician K-bentonites: A new stratigraphic tool. Geology, 22, 115–118.

Devine, J.D., Gardner, J.E., Brack, H.P., Layne, G.D., and Rutherford, M.J. (1995) Comparison of microanalytical methods for estimating H_2O contents of silicic volcanic glasses. American Mineralogist, 80, 319–328.

Dunbar, N.W., Hervig, R.L., and Kyle, P.R. (1989) Determination of pre-eruptive H_2O, F, and Cl contents of silicic magmas using melt inclusions: Examples from the Taupo Volcanic Center. Bulletin of Volcanology, 51, 177–184.

Dunbar, N.W., and Hervig, R.L. (1992a) Petrogenesis and volatile stratigraphy of the Bishop Tuff: Evidence from melt inclusion analysis. Journal of Geophysical Research, 97, 15129–15150.

——— (1992b) Volatile and trace element composition of melt inclusions from the lower Bandelier Tuff: Implications for magma chamber processes and eruptive style. Journal of Geophysical Research, 97, 15151–15170.

Dunbar, N.W., and Kyle, P.R. (1993) Lack of volatile gradient in the Taupo plinian-ignimbrite transition: Evidence from melt inclusion analysis. American Mineralogist, 78, 612–618.

Hanson, B., von Kiparski, W., and Delano, J.W. (1992a) Petrology and geochemistry of melt inclusions within quartz phenocrysts from Paleozoic K-bentonites. Geological Society of America Abstracts with Programs, 24, 176.

Hanson, B., Delano, J.W., von Kiparski, W., and Schirnick, C. (1992b) The occurrence of melt inclusions in quartz phenocrysts from K-bentonites in the Helderberg Group of New York State and their potential use in stratigraphic correlation. Geological Society of America Abstracts with Programs, 24, 27.

Haynes, J.T. (1994) The Ordovician Deike and Millbrig K-bentonite beds of the Cincinnati Arch and the southern Valley and Ridge Province. Geological Society of America Special Paper, 290, 80 p.

Haynes, J.T., Melson, W.G., and Kunk, M.J. (1995) Composition of biotite phenocrysts in Ordovician tephras casts doubt on the proposed trans-Atlantic correlation of the Millbrig K-bentonite (United States) and the Kinnehulle bentonite (Sweden). Geology, 23(9), 847–850.

Hervig, R.L., Dunbar, N., Westrich, H.R., and Kyle, P.R. (1989) Pre-eruptive water content of rhyolitic magmas as determined by ion microprobe analyses of melt inclusions in phenocrysts. Journal of Volcanology and Geothermal Research, 36, 293–302.

Hervig, R.L., and Dunbar, N.W. (1992) Cause of chemical zoning in the Bishop (California) and Bandelier (New Mexico) magma chambers. Earth and Planetary Science Letters, 111, 97–108.

Huff, W.D. (1983) Correlation of Middle Ordovician K-bentonites based on chemical fingerprinting. Journal of Geology, 91, 657–669.

Huff, W.D., and Kolata, D.R. (1989) Correlation of K-bentonite beds by chemical fingerprinting using multivariate statistics, p. 567–577. In T.A. Cross, Ed., Quantitative dynamic stratigraphy. Prentice Hall, Englewood Cliffs, New Jersey.

Izett, G.A. (1981) Volcanic ash beds: Recorders of Upper Cenozoic silicic pyroclastic volcanism in the western United States. Journal of Geophysical Research, 86, 10200–10222.

Jercinovic, M.J., and Keil, K. (1988) Electron microprobe analyses of basaltic glasses and associated alteration products. Microbeam Analyses, 23, 495–497.

Karsten, J.L., Holloway, J.R., and Delaney, J.R. (1982) Ion microprobe studies of water in silicate melts: Temperature-dependent water diffusion in obsidian. Earth and Planetary Science Letters, 59, 420–428.

Kilinc, A., Carmichael, I.S.E., Rivers, M.L., and Sack, R.O. (1983) The ferric-ferrous ratio of natural silicate liquids equilibrated in air. Contributions to Mineralogy and Petrology, 83, 136–140.

Lindstrom, D.J. (1990) Analysis of submicrogram samples by INAA. Nuclear Instruments and Methods in Physics Research, A299, 584–588.

Lindstrom, D.J., and Korotev, R.L. (1982) TEABAGS: Computer programs for instrumental neutron activation analysis. Journal of Radioanalytical Chemistry, 70, 439–458.

Lu, F., Anderson, A.T., and Davis, A.M. (1992) Melt inclusions and crystal-liquid separation in rhyolitic magma of the Bishop Tuff. Contributions to Mineralogy and Petrology, 110, 113–120.

Lyons, P.C., Outerbridge, W.F., Triplehorn, D.M., Evans, H.T., Congdon, R.C., Capiro, M., Hess, J.C., and Nash, W.P. (1992) An Appalachian isochron: A kaolinitized carboniferous air-fall volcanic-ash deposit (tonstein). Geological Society of America Bulletin, 104, 1515–1527.

Mitchell, C.M., Goldman, D., Delano, J.W., Samson, S.D., and Bergström, S.M. (1994) Temporal and spacial distribution of biozones and facies relative to geochemically correlated K-bentonites in the Middle Ordovician Taconic foredeep. Geology, 22, 715–718.

Newman, S., Stolper, E.M., and Epstein, S. (1986) Measurement of water in rhyolitic glasses: Calibration of an infrared spectroscopic technique. American Mineralogist, 71, 1527–1541.

Newman, S., Epstein, S., and Stolper, E.M. (1988) Water, carbon dioxide, and hydrogen isotopes in glasses from the ca. 1340 A.D. eruption of the Mono Craters, California: Constraints on degassing phenomena and initial volatile content. Journal of Volcanology and Geothermal Research, 35, 75–96.

Nielsen, C.H., and Sigurdsson, H. (1981) Quantitative methods for electron microprobe analysis of sodium in natural and synthetic glasses. American Mineralogist, 66, 547–552.

Payette, C., and Martin, R.F. (1986) The Harvey Volcanic Suite, New Brunswick: 1. Inclusions of magma in quartz phenocrysts. Canadian Mineralogist, 24, 557–570.

Rowley, D.B., and Kidd, W.S.F. (1981) Stratigraphic relationships and detrital composition of the medial Ordovician flysch of western New England: Implications for the tectonic evolution of the Taconic orogeny. Journal of Geology, 89, 199–218.

Rutherford, M.J., Sigurdsson, H., Carey, S., and Davis, A. (1985) The

May 18, 1980 eruption of Mount St. Helens: 1. Melt composition and experimental phase equilibria. Journal of Geophysical Research, 90, 2929–2947.

Rutherford, M.J., and Devine, J.D. (1993) Pre-eruption *P-T* conditions and volatiles in the 1991 Pinatubo magma. In Geological Society of America Special Publication.

Samson, S.D., Matthews, S., Mitchell, C.E., and Goldman, D. (1995) Tephrochronology of highly altered ash beds: The use of trace element and strontium isotope geochemistry of apatite phenocrysts to correlate K-bentonites. Geochimica et Cosmochimica Acta, 59, 2527–2536.

Sardeson, F.W. (1928) Bentonite seams in stratigraphic correlation. Pan-American Geologist, 50, 107–116.

Schirnick, C. (1990) Origin, sedimentary geochemistry, and correlation of Middle and Late Ordovician K-bentonites: Constraints from melt inclusions and zircon morphology. Masters dissertation, State University of New York at Albany.

Sommer, M.A. (1977) Volatiles, H_2O, CO_2, and CO in silicate melt inclusions in quartz phenocrysts from the rhyolitic Bandelier air-fall and ash-flow tuff, New Mexico. Journal of Geology, 85, 423–432.

Sommer, M.A., and Schramm, L.S. (1983) An analysis of the water concentrations in silicate melt inclusions in quartz phenocrysts from the Bandelier Tuff, Jemez Mts, New Mexico. Bulletin Volcanologique, 46, 299–320.

Stolper, E.M. (1982) Water in silicate glasses: An infrared spectroscopic study. Contributions to Mineralogy and Petrology, 81, 1–17.

Takenouchi, S., and Imai, H. (1975) Glass and fluid inclusions in acidic igneous rocks from some mining areas in Japan. Economic Geology, 70, 750–769.

Webster, J.D., and Duffield, W.A. (1991) Volatiles and lithophile elements in the Taylor Creek Rhyolite: Constraints from glass inclusion analysis. American Mineralogist, 76, 1628–1645.

Webster, J.D., Congdon, R.D., and Lyons, P.C. (1995) Determining pre-eruptive compositions of Late Paleozoic magma from Kaolinized volcanic ashes: Analysis of glass inclusions in quartz microphenocrysts from tonsteins. Geochimica et Cosmochimica Acta, 59, 711–720.

Manuscript received June 14, 1995
Manuscript accepted June 5, 1996